J Mater Sci
DOI 10.1007/s10853-010-4907-4

Morphologies and optical properties of nanostructures self-assembled from asymmetrical, amphiphilic perylene derivatives

Xin Yang · Xiaohe Xu · Yanqing Lu · Hai-Feng Ji · Sheng Dai

Received: 25 July 2010 / Accepted: 6 September 2010

Abstract Two asymmetrical, amphiphilic perylene derivatives, *N*-Decyl-perylene-3,4:9,10-tetracaboxylic-3,4-di(methoxyethoxyethyl)ester-9,10-imide (**D1E2**) and *N*-(1-Decylundecyl)-perylene-3,4:9,10-tetracaboxylic-3,4-di(methoxyethoxyethyl)ester-9,10-imide (**D2E2**), have been synthesized and characterized. These compounds contain one long hydrophobic chain on one end and two hydrophilic ethoxy chains on the other end. Self-assembly of these molecules in a variety of solvents has been demonstrated. Scanning electron microscopy images showed that these compounds self-assembled to various nanostructures in different solvents. The most well-defined structure was flexible nanoribbons obtained from **D1E2** precipitation in methanol. The UV–vis absorption and fluorescence spectra of these compounds in solution and solid form are also reported. The self-assembled nanostructures have potential applications in optoelectronics.

Introduction

Self-assembly of organic molecules in solutions represents an important bottom-up approach in designing electronic and optoelectronic devices [1]. The applications include optical elements, memory elements, electro-optic cells, actuators, sensors, etc. Bendikov et al. [2]. Understanding the noncovalent interaction mechanisms will help to design and synthesize molecules for the fabrication of efficient devices. Among the organic molecules, aromatic compounds have been known for the formation of one-dimensional (1D) nanostructures through strong interactions [3–17]. Particularly, perylene tetracarboxylic bisimide derivatives are of interest because of their n-type characteristics [8, 14]. Most of the reported nanoassemblies of perylene tetracarboxylic bisimide derivatives were symmetrical [8–17].

Recently, asymmetrical perylene tetracarboxylic bisimide derivatives have attracted more interests [18–20]. When the two side chains have different hydrophobic/hydrophilic characteristics, the morphology of the nanoassembly is expected to be controlled by both the structures of the side chains and the solvents. In this study, we report self-assembled nanostructures of two asymmetrical, amphiphilic perylene derivatives that bear one hydrophobic chain at one side, and two hydrophilic ethoxy chains at the other. One compound self-assembles into long, flexible, well-defined nanoribbons in methanol and the other forms nanoparticles. The spectroscopic behaviors of these compounds are also studied.

Electronic supplementary material The online version of this article (doi:10.1007/s10853-010-4907-4) contains supplementary material, which is available to authorized users.

X. Yang · X. Xu · H.-F. Ji (✉)
Department of Chemistry, Drexel University, Philadelphia, PA 19010, USA
e-mail: hj56@drexel.edu

Y. Lu
Institute for Micromanufacturing, Louisiana Tech University, Ruston, LA 71272, USA

S. Dai
Chemical Sciences Division, Oak Ridge National Laboratory, Oak Ridge, TN 37831, USA

Journal : Large 10853 | Dispatch : 15-9-2010 | Pages : 8
Article No. : 4907 | LE | TYPESET
MS Code : JMSC19264 | CP | DISK

Experimental

Instruments

UV–vis absorption spectra were recorded by use of a Shimadzu UV-2401PC spectrophotometer, with temperature control (CPS-Controller). Fluorescence spectra were obtained using a Hitachi F-2500 fluorescence spectrometer. In all the fluorescence experiments, the molecules were excited at 470 nm. Proton nuclear magnetic resonance spectra were recorded on a GSX FTNMR Spectrometer (JEOL JNM-GSX270 FTNMR). The mass spectrum was obtained with a JEOL AccuTOF-DART^{TM} system. The temperature for the orifice 1 was set at 80 °C, direct analysis in real time (DART) temperature was set at 300 °C. The orifice 1 voltage, orifice 2 voltage, and ring lens voltage were 20, 3, and 3, respectively. Helium was used as DART working gas, and flow rate was set at 5.6 L/min. The DART needle voltage was 3500 V, and the electrode #1 and #2 voltages were 150 and 250, respectively. Hitachi FESEM S4800 was used to obtain scanning electron microscopy (SEM) images. JOEL 2200 FS was used for obtaining transmission electron microscopy (TEM) images.

Materials and synthesis

Scheme 1 shows the synthetic route of the two asymmetrically substituted amphiphilic perylene derivatives, **D1E2** and **D2E2**. 2-(2-Methoxyethoxy)ethyl iodide was synthesized according to a reported method [21, 22]. Perylene monoimide *N*-(1-Decyl-perylene)-3,4:9,10-tetracaboxylic-3,4-anhydride-9,10-imide (**1a**) [15, 22] and *N*-(1-Decylundecyl)-perylene-3,4:9,10-tetracarboxylic-3,4-anhydride-9,10-imide (**1b**) [23] were synthesized according to reported procedures. All the synthesized compounds were characterized by ^{1}H NMR spectroscopy and mass spectrometry. All the chemicals were purchased from Aldrich (Milwaukee, MI, USA) without further purification.

N-Decyl-perylene-3,4:9,10-tetracaboxylic-3,4-di(methoxyethoxyethyl)ester-9,10-imide (**2a** or **D1E2**).

D1E2 was synthesized from compound **1** with the corresponding alcohol and alkyl iodide according to a modified method [15]. A mixture of **1a** (100 mg, 0.188 mmol, $C_{34}H_{29}NO_5$), 2-(2-Methoxyethoxy) ethanol (0.16 g, 1.34 mmol), 2-(2-Methoxyethoxy) ethyl iodide (0.29 g, 1.27 mmol), and potassium carbonate (100 mg, 0.72 mmol) was heated at 70 °C for 1 day. The excess of iodide and alcohol was distilled under reduced pressure. The residue was diluted in a 15 mL of deionized water, and then filtered, further dried under reduced pressure in a desiccator, and recrystallized from methanol to afford 122 mg (86.2%) of an orange red solid. The melting point of **D1E2** was 194–195 °C. Elemental analysis, expected: C 70.10%, H 6.82%, O 21.22%; Observed: C 70.22%, H 6.74%, O 21.48%; $C_{44}H_{51}NO_{10}$, MS (*m/z*):753.35 (M^+, 20.4%), 754.35 [$(M + 1)^+$, 100%], 755.35 [$(M + 2)^+$, 40.7%]. ^{1}H NMR($CDCl_3$) 8.64 (2H, J = 7.9 perylene), 8.48 (4H, J = 9.0, perylene), 8.14 (2H, J = 7.9 perylene), 4.50 (t, 4H, COO–CH_2, J = 4.9), 4.20 (t, 2H, N–CH_2, J = 7.2), 3.88–3.54 (m, 12H, O–CH_2), 3.37 (s, 6H, OCH_3), 1.55–1.25 (m, 16H, CH_2), 0.85 (t, 3H, CH_3, J = 6.7).

N-(1-Decylundecyl)-perylene-3,4:9,10-tetracaboxylic-3,4-di(methoxyethoxyethyl)ester-9,10-imide (**2b** or **D2E2**).

A mixture of **1b** (200 mg, 0.321 mmol, $C_{45}H_{51}NO_5$), 2-(2-Methoxyethoxy) ethanol (0.2828 g, 2.3 mmol), 2-(2-Methoxyethoxy) ethyl iodide (0.4981 g, 2.17 mmol), and potassium carbonate (0.1261 g, 0.91 mmol) was heated at 70 °C for 1 day. The excess of iodide and alcohol was distilled under reduced pressure. The product was re-crystallized from methanol to afford 260 mg of brown red solid (89%). The compound **D2E2** was identified by MS and NMR. ^{1}H NMR($CDCl_3$) 8.62–8.14 (m, 8H, perylene), 4.50 (t, 2H, COO–CH_2), 5.20 (m, 1H, N–CH), 3.90–3.58 (m, 12H, O–CH_2), 3.40 (s, 6H, O–CH_3), 1.85–1.12 (m, 36H, CH_2), 0.81 (t, 6H, –CH_3). $C_{55}H_{73}NO_{10}$, MS (*m/z*): 908.53 (M^+, 100%), 909.53 [$(M + 1)^+$ 53.0%], 910.53 [$(M+2)^+$, 22.8%].

Scheme 1 The synthetic route of **D1E2** and **D2E2**

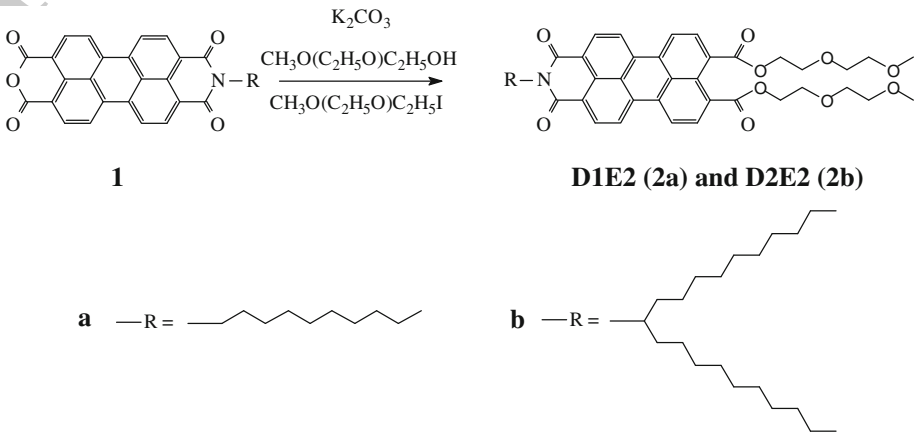

Journal : Large 10853 | Dispatch : 15-9-2010 | Pages : 8
Article No. : 4907 | LE | TYPESET
MS Code : JMSC19264 | CP | DISK

Results and discussion

Optical properties of D1E2 and D2E2 in solutions

D1E2 dissolves in CH_2Cl_2, tetrahydrofuran (THF), and toluene at a concentration as high as 10^{-3} M, but has a relatively lower solubility in MeOH and hexane. The UV–vis and fluorescence spectra of **D1E2** in different solvents at low concentration, under which π–π stacking behavior does not occur, are shown in Fig. 1. In UV–vis spectra (Fig. 1 left), **D1E2** shows a red shift in the toluene solution, and a blue shift in the hexane solution because of different energy levels of the excited state of the perylene moieties. These can be readily explained that in nonpolar solvents such as hexane the excited state of the perylene moiety has a relative higher energy than that in polar solvents; and in toluene, the excited state of the perylene moiety can be stabilized by forming weak perylene/toluene complexes [24].

The UV–vis absorption and fluorescence spectra of **D1E2** in toluene, THF, and CH_2Cl_2 do not show changes in optical properties, except for intensity, on concentration variation between 10^{-8} and 10^{-3} M. The UV and fluorescence spectra of the **D1E2** in hexane are independent of concentration when the concentration is lower than 10^{-6} M. Precipitates are observed when the concentration is above 10^{-6} M. In methanol, however, **D1E2** forms H-type aggregates in the clear solutions when the concentration is higher than 5×10^{-4} M. This is manifested by the fact that the maximum absorption band of **D1E2** is blue shifted from 497 to 470 nm (Fig. 2a), i.e., there is a change in the ratio of the intensities of the 0–0/0–1 peak, which is typical of H-type aggregation [25–28]. No observation was made on slipped J-type aggregates, which is typically accompanied by red shift of absorption bands of the chromophores when the concentration increases [29]. The formation of H-aggregates is further confirmed by the transition electron microscopy images that will be discussed in Sect. Structure analysis of D1E2 nanoribbons precipitated from methanol in this article. Aggregation behavior of **D1E2** in methanol occurs above 1×10^{-4} M is also shown from fluorescence spectra (Fig. 2b) of **D1E2**. The new peak at 1×10^{-4} and 5×10^{-4} M is at approximately 555 nm, and further red shifts to 585 nm at 1×10^{-3} M with a diminished peak, an indicative of H-aggregation as well. When the concentration is lower than 1×10^{-5} M, no aggregation peaks were observed; however, the fluorescence versus concentration showed a deviation from linearity, which is due to the inner filter effect and re-absorption [30, 31]. The UV and fluorescence spectra in THF:H_2O (1:1) and methanol:H_2O (1:1) are similar to those in methanol.

The UV and fluorescence properties of **D2E2** in solvents at low concentrations (Fig. 3a) are similar to those of **D1E2** (Fig. 1). The UV and fluorescence properties of **D2E2** at higher concentrations have showed that **D2E2** does not form H-aggregate in methanol (Fig. 3b), THF:H_2O, and Methanol:H_2O.

Optical properties of D1E2 and D2E2 in the solid state

D1E2 precipitations are observed when the concentrations are greater than 1×10^{-6}, 2×10^{-3}, 2×10^{-5}, and 5×10^{-6} M in hexane, methanol, THF:H_2O (1:1), and MeOH:H_2O(1:1), respectively. The solids that are precipitated from these solvents are transferred to a quartz plate for UV–vis absorption and on a gold-coated substrate for image analysis. Other solid samples prepared from evaporation of a drop of **D1E2** solution in CH_2Cl_2, THF, and toluene, respectively, on the substrates, are also analyzed for comparison. The UV–vis absorption spectra (Fig. 4a) of these solids are quite similar to each other with the 0–0/0–1 ratio less than 1 and a new peak at approximately 550 nm, indicating the aggregation of **D1E2** in the solid state. Figure 4b shows the fluorescence spectra of the solid samples evaporated from solvents in comparison with solid

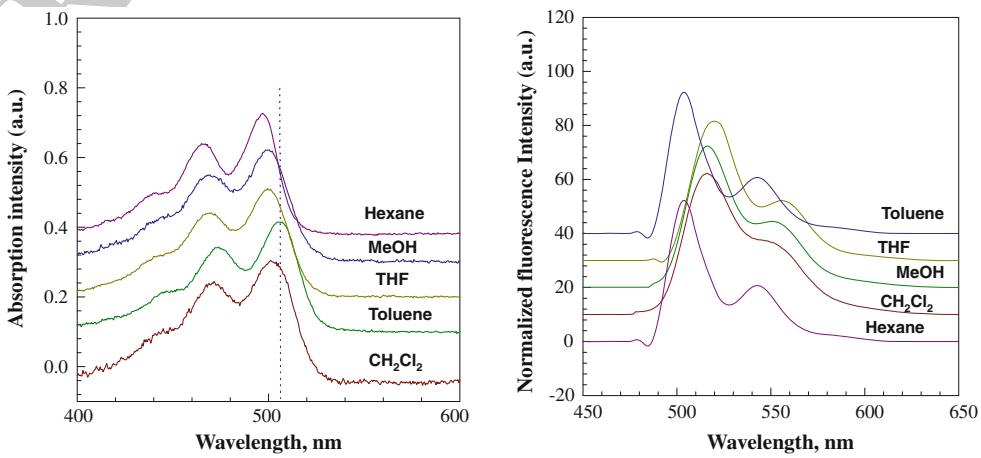

Fig. 1 UV–vis absorption (*left*) and fluorescence (*right*) spectra of 10^{-7} M **D1E2** at 20 °C in hexane, toluene, CH_2Cl_2, MeOH, and THF. Both spectra are normalized at the 0–1 transition maximum

Journal : Large 10853 Dispatch : 15-9-2010 Pages : 8
Article No. : 4907 LE TYPESET
MS Code : JMSC19264 CP DISK

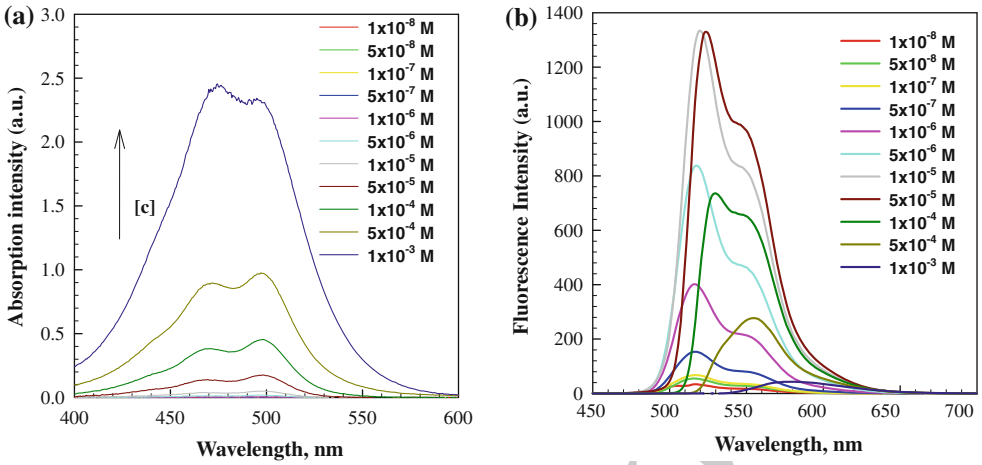

Fig. 2 UV–vis absorption **a** and fluorescence **b** spectra of **D1E2** in methanol. The concentration varied between 1×10^{-8} and 1×10^{-3} M

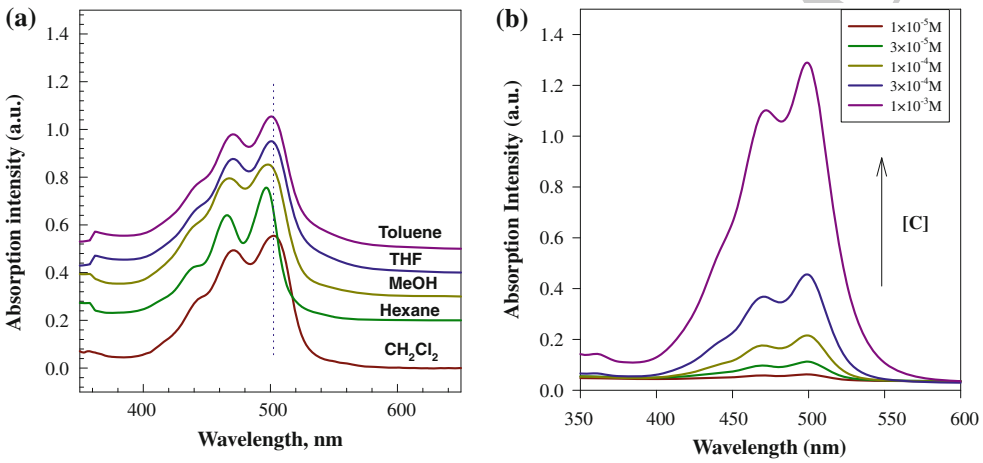

Fig. 3 **a** UV–vis absorption spectra of 10^{-7} M **D2E2** at 20 °C in hexane, toluene, CH_2Cl_2, MeOH, and THF. **b** UV–vis absorption spectra of **D2E2** in methanol. The concentration varied between 1×10^{-5} and 1×10^{-3} M

samples precipitated from hexane, methanol, THF:H_2O, and methanol:H_2O. The fluorescence spectrum of the sample from methanol shows a broad emission band at approximately 610 nm corresponding to the emission from the H-aggregates, and all the monomer peaks disappear, suggesting a strong π–π stacking and a typical H-type aggregation behavior [23]. Fluorescence spectra from all other solid samples show both monomer peaks and a shoulder peak at approximately 610 nm, indicating the existence of both monomers and aggregates in these samples.

The UV–vis absorption and fluorescence spectra of **D2E2** (Figure not shown) are similar to those of **D1E2** except that both monomer and aggregation peaks exist in the fluorescence spectra from samples precipitated from various solvents, including methanol.

SEM images of the D1E2 and D2E2 nanostructures

The solid-state **D1E2** aggregate was investigated using SEM. Figure 5 shows the aggregation variations of the solid samples from different solvents. The solid sample from evaporation of CH_2Cl_2 on the substrate shows a particle-fused film character (Fig. 5a). Others solid samples from evaporation of THF and toluene are similar to this film morphology. The solids precipitated from hexane (Fig. 5b), MeOH:H_2O (1:1, Fig. 5c), and THF:H_2O (1:1, Fig. 5d) are in the form of particle, star, and curled-hairs shape, respectively. The solid precipitated from methanol showed the most ordered shape (Fig. 6). The SEM images demonstrated the millimeter-long, flexible, and well-defined nanoribbons of **D1E2** precipitated from methanol. These results show that the solvents could significantly affect the morphology of these nanostructures. Ordered nanostructures of **D1E2** are only formed from polar protic solvents, which might be attributed to the dominant polar ethoxy groups. This is consistent with reports that perylene derivatives bearing hydrophobic chains form well-organized nanowire structures in nonpolar solvents [9, 10], and perylene derivatives bearing hydrophilic chains form well-organized nanostructures in polar solvents [9]. The

Journal : Large 10853 Dispatch : 15-9-2010 Pages : 8
Article No. : 4907 LE TYPESET
MS Code : JMSC19264 CP DISK

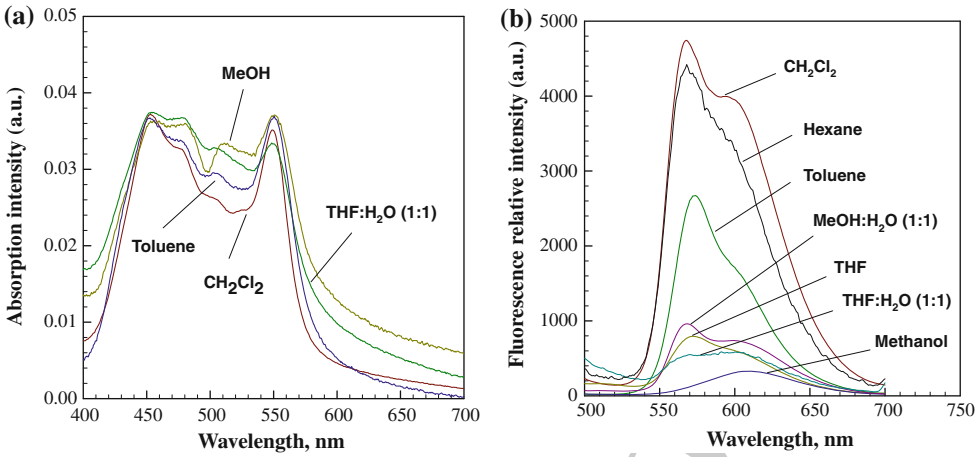

Fig. 4 **a** UV–vis absorption. **b** Fluorescence spectra of solids samples prepared from evaporation of **D1E2** from toluene, THF, and CH_2Cl_2 and precipitation from MeOH, hexane, THF:H_2O (1:1), and MeOH:H_2O (1:1)

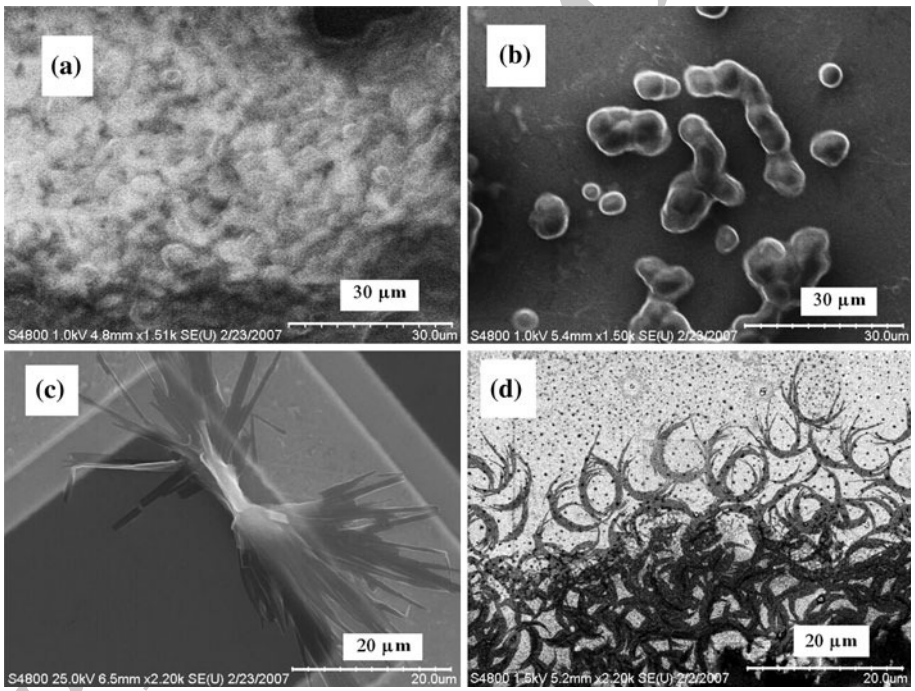

Fig. 5 SEM images of **D1E2** solids **a** evaporated from CH_2Cl_2, **b** precipitated from hexane, **c** precipitated from MeOH:H_2O (1:1), and **d** precipitated from THF:H_2O (1:1)

fact that **D1E2** does not form long nanowires in organic-H_2O binary solvents might due to hydrophobic effect, which competes with the π–π interaction between perylene moieties.

The nanoribbons that precipitated from 5×10^{-3} M of **D1E2** in methanol were 200 to 2 μm in width, approximately 40 to 100 nm in thickness (Fig. 6a, b). The nanoribbons are flexible. This fact that well-ordered nanostructure only occurred on solids precipitated from methanol was consistent with the spectroscopic results that only in these solid samples, all the monomer peaks disappeared, suggesting strong π–π stacking and a typical H-type aggregation behavior. The width and thickness of the nanoribbons do not increase when **D1E2** is precipitated from higher concentrations in methanol (1×10^{-2} to 1×10^{-1} M), but aggregates to bundles (Fig. 6c). Figure 6d shows layered thin nanostrips at the end of a typical nanoribbon nanoassembly, indicating that the **D1E2** firstly aggregates to thin nanostrips and then further self-assembles into layered structure.

D2E2 solids precipitated or evaporated from the above five organic solvents show film characteristic as shown in Fig. 7a and b. The solids precipitated from MeOH:H_2O (1:1, Fig. 7c) and THF:H_2O (1:1, Fig. 7d) show particles structures and no well-ordered morphology as those of **D1E2** were observed. The side effect on the self-assembly has been discussed previously on symmetrical molecules [9, 10], and it was concluded that perylene moieties with swallow-tail-like chains could not stacked into well-ordered nanofibers because of the significant steric

Journal : Large 10853 Dispatch : 15-9-2010 Pages : 8
Article No. : 4907 LE TYPESET
MS Code : JMSC19264 CP DISK

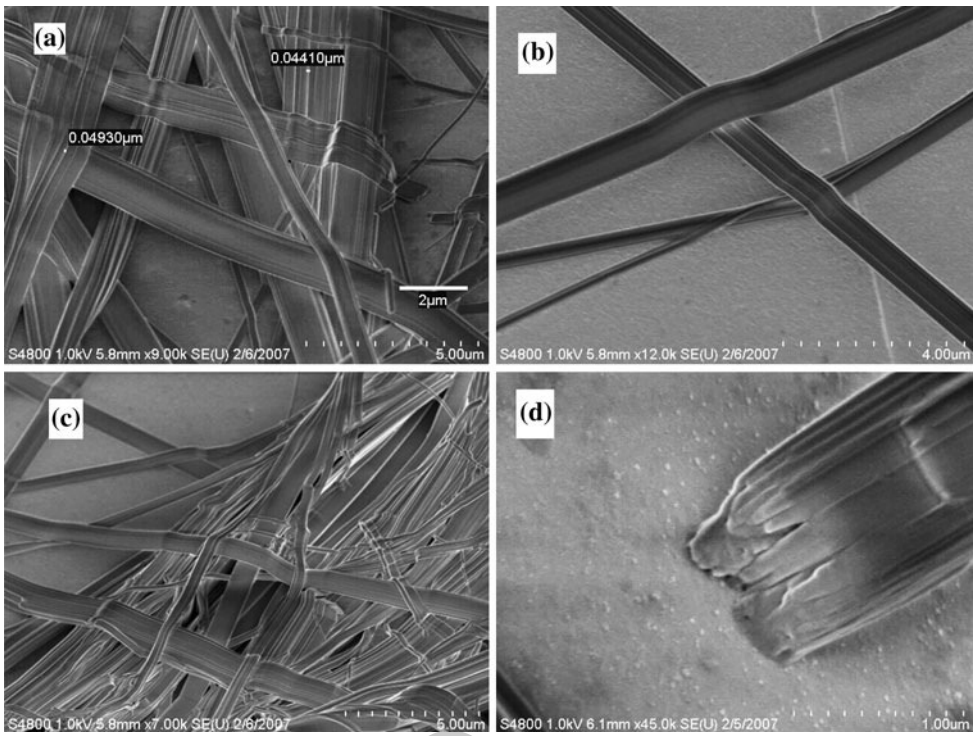

Fig. 6 SEM images of **a** and **b D1E2** nanoribbons precipitated from MeOH at 5×10^{-3} M, **c** nanoribbons precipitated from MeOH at 2×10^{-2} M, and **d** the end of a nanoribbon with layered nanostripes

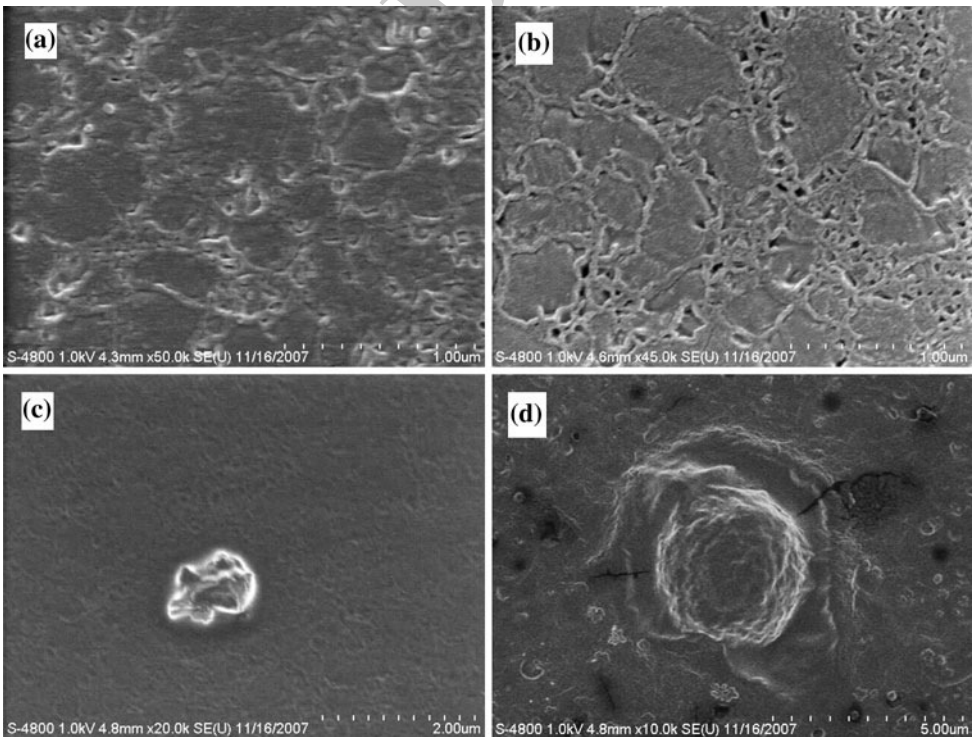

Fig. 7 SEM images of **D2E2** solids, **a** precipitated from a MeOH solution, **b** evaporated from a THF solution, **c** precipitated from a MeOH:H_2O (1:1) solution, and **d** precipitated from THF:H_2O (1:1) solution

hindrance. Our observations on **D2E2** and the comparison with **D1E2** agree with this assumption and we demonstrate that asymmetrical amphiphilic perylene derivative **D2E2** with one swallow-tail-like chain has the similar behavior as those symmetrical ones [9, 10].

Structure analysis of D1E2 nanoribbons precipitated from methanol

Transmission electron microscopy experiments show that the **D1E2** nanoribbons (Fig. 8) have a crystalline

Journal : Large 10853 | Dispatch : 15-9-2010 | Pages : 8
Article No. : 4907 | LE | TYPESET
MS Code : JMSC19264 | CP | DISK

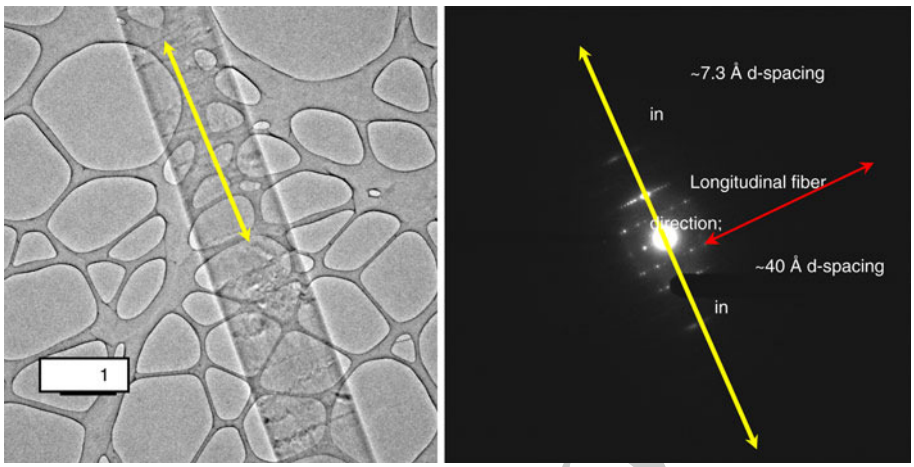

Fig. 8 TEM image (*left*) and electron diffraction pattern (*right*) of a **D1E2** nanoribbon

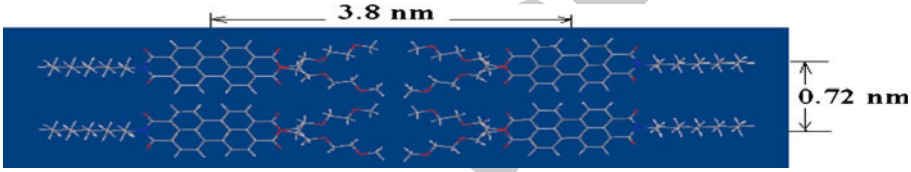

Scheme 2 Model of the distance between two **D1E2** molecules in the nanobelt

structure and the ribbon exhibited diffuse "texture" in the longitudinal direction. The corresponding electron diffraction pattern (Fig. 8 bottom) shows well-defined diffraction spots with 7.3 Å characteristic d-spacing in the longitudinal direction and 42 Å d-spacing in the perpendicular nanoribbon direction, which suggests that the molecules are oriented with their long axis (x axis) perpendicular to the ribbon direction and the shoulder-to-shoulder axis (y axis) parallel to the ribbon direction, respectively, as shown in Scheme 2, modeled by the Chem3D software. The modeled d-spacing are 38 Å in the perpendicular direction and 7.2 Å in the longitudinal direction, which are slightly smaller than those measured.

Conclusions

In summary, we showed supramolecular stacks of two asymmetrical, amphilphilic perylene derivatives, **D1E2** and **D2E2**, in a variety of solvents or solvent mixtures. Our study showed that the assembly of artificial heterogeneous molecular systems could be controlled by both solvent and the side chains. Potential applications of these nanowires include optoelectronics, nanoelectronics, and light emitting devices. We are currently exploring fundamental understanding of the nanoelectronic properties and functionality of these supramolecular nanostructures, which is essential for developing their potential as the building blocks of future nanoscale devices.

References

1. Green JE, Choi JW, Boukai A, Bunimovich Y, Johnston-Halperin E, Delonno E, Luo Y, Sheriff BA, Xu K, Shin YS, Tseng HR, Stoddart JF, Health JR (2007) Nature 445:414
2. Bendikov M, Wudl F, Perepichka DF (2004) Chem Rev 104:4891
3. Duzhko V, Singer KD (2007) J Phys Chem C 111:27
4. Hill JP, Jin W, Kosaka A, Fukushima T, Ichihara H, Shimomura T, Ito K, Hashizume T, Ishii N, Aida T (2004) Science 304:1481
5. Briseno AL, Mannsfeld SCB, Lu X, Xiong Y, Jenekhe SA, Bao Z, Xia Y (2007) Nano Lett 7:668
6. Glusen K, Singer D, Kohne B, Ebert M, Liebmann A, Wendorff JH (1991) Liq Cryst 10:147
7. Tang Q, Li H, He M, Hu W, Liu C, Chen K, Wang C, Liu Y, Zhu D (2006) Adv Mater 18:65
8. Balakrishnan K, Datar A, Oitker R, Chen H, Zuo J, Zang L (2005) J Am Chem Soc 127:10496
9. Balakrishnan K, Datar A, Naddo T, Huang J, Otiker R, Yen M, Zhao J, Zang L (2006) J Am Chem Soc 128:7390
10. Wicklein A, Lang A, Muth M, Thelakkat M (2009) J Am Chem Soc 131:14442
11. Sinks LE, Rybtchinski B, Iimura M, Jones BA, Goshe AJ, Zuo X, Tiede DM, Li X, Wasielewski MR (2005) Chem Mater 17:6295
12. Gesquiere A, Jonkheijm P, Hoeben FJM, Schenning APHJ, De Feyter S, De Schryver FC, Meijer EW (2004) Nano Lett 4:1175
13. Schenning APH, Herrikhuyzen JV, Jonkheijm P, Chen Z, Würthner F, Meijer EW (2002) J Am Chem Soc 124:10252
14. Xu BQ, Xiao X, Yang X, Zang L, Tao NJ (2005) J Am Chem Soc 127:2386
15. Arnaud A, Belleney J, Boué F, Bouteiller L, Carrot G, Wintgens V (2004) Angew Chem Int Ed 43:1718
16. Jones BA, Ahrens MJ, Yoon M-H, Marks TJ, Wasielewski MR (2004) Angew Chem Int Ed 43:6523
17. Hernando J, de Witte PAJ, van Dijk EMHP, Korterik J, Nolte RJM, Rowan AE, García-Parajó MF, van Hulst NF (2004) Angew Chem Int Ed 43:4045
18. Che Y, Datar A, Yang X, Naddo T, Zhao J, Zang L (2007) J Am Chem Soc 129:6354

Journal : Large 10853 | Dispatch : 15-9-2010 | Pages : 8
Article No. : 4907 | LE | TYPESET
MS Code : JMSC19264 | CP | DISK

19. Zhang X, Chen Z, Wurthner F (2007) J Am Chem Soc 129:4886
20. Yang X, Xu X, Ji H-F (2008) J Phys Chem B 112:7196
21. Prugh JD, Hartman GD, Mallorga PJ, McKeever BM, Michelson SR, Murcko MA, Schwam H, Smith RL, Sondey JM (1991) J Chem Med 34:1805
22. Brunsveld L, Zhang H, Glasbeek M, Vekemans JAJM, Meijer EW (2000) J Am Chem Soc 122:6175
23. Kaiser H, Lindner J, Langhals H (1991) Chem Ber 124:529
24. Joireman PW, Connell LL, Ohline SM, Felker PM (1991) Chem Phys Lett 182:385
25. Wurthner F, Chen Z, Dehm V, Stepanenko V (2005) Chem Comm 1188
26. Wurthner F, Thalacker C, Diele S, Tschierske C (2001) Chem Eur J 7:2245
27. Wang W, Han JJ, Wang L-Q, Li L-S, Shaw WJ, Li ADQ (2003) Nano Lett 3:455
28. Neuteboom EE, Meskers SCJ, Meijer EW, Janssen RAJ (2004) Macromol Chem Phys 205:217
29. Beckers EHA, Chen Z, Meskers SCJ, Jonkheijm P, Schenning APHJ, Li X-Q, Osswald P, Wurthner F, Jassen RAJ (2006) J Phys Chem 110:16967
30. Kufazvinei C, Ruether M, Wang J, Blau W (2009) Org Electron 10:674
31. Rickard D, Giordani S, Blau WJ, Coleman JN (2008) J Lumin 128:31

Journal : Large 10853 | Dispatch : 15-9-2010 | Pages : 8
Article No. : 4907 | ☐ LE | ☐ TYPESET
MS Code : JMSC19264 | ☑ CP | ☑ DISK